

# Femtosecond Pulse Shaping with Plasmonic Crystals<sup>†</sup>

P. P. Vabishchevich, M. R. Shcherbakov, V. O. Bessonov, T. V. Dolgova, and A. A. Fedyanin

*Faculty of Physics, Moscow State University, Moscow, 119991 Russia*

*e-mail: fedyanin@nanolab.phys.msu.ru*

Received May 18, 2015

The temporal shaping of femtosecond laser pulses reflected from a one-dimensional plasmonic crystal using a commercially available polymer grating coated with a silver film is experimentally demonstrated by time-resolved measurements of the intensity correlation function. Shaping is achieved by the excitation of surface plasmon-polaritons with a lifetime comparable to the 130 fs laser pulse duration. The variety of data obtained demonstrate the flexible shaping of fs-pulses by delaying, advancing, splitting, broadening, compressing, and changing the topological properties of the pulse with the plasmonic crystals under study.

DOI: 10.1134/S0021364015120140

## 1. INTRODUCTION

Femtosecond laser pulse shaping technology [1, 2] has found many applications in fundamental science and applied research, e.g., in studies of light-matter interaction [3], the coherent control of quantum states [4, 5], all-optical switching [6], biomechanical and biomedical applications [7, 8], and optical communications [9–11]. All these applications require maximal flexibility in the design of femtosecond pulse electric fields. The Fourier transform pulse shaping technique [12, 13] involves a spatial light modulator placed in the plane of symmetry of a  $4f$ -zero-dispersion compressor, which modifies the individual frequency components of the spectrally dispersed pulse. The direct space-to-time pulse shaping is also propitious for communication applications [14–16]. Another approach is pulse reshaping by light-matter interactions [17, 18]. The main idea behind this approach is the use of ultrafast processes with durations of a few hundreds of femtoseconds, which can be temporally mixed with femtosecond laser pulses. The use of surface waves in the temporal reshaping of femtosecond pulses was theoretically suggested in [19]. The earliest experimental works reported a femtosecond pulse delay induced by resonant surface plasmon-polariton (SPP) excitation [20, 21]. Later on, temporal pulse reshaping was demonstrated experimentally [22–25]. These pulse modifications strongly depend on the interplay between the parameters of the fs-pulse and SPP resonance. For example, in plasmonic crystals [26, 27], the SPP lifetime varies from several tens of femtoseconds to several picoseconds in the spectral vicinity of a plasmonic band gap (PBG). Significant differences in the nature of the fs-pulse distortion were found for the SPP states at two PBG edges, resulting in a sharp contrast in their lifetimes [28, 29]. In this paper, the controllable

reshaping of a femtosecond laser pulse reflected from a digital versatile disc (DVD)-based plasmonic crystal is reported. The reshaping of fs-pulses is demonstrated by time-resolved measurements of the intensity correlation functions. Various pulse-shaping options, namely, broadening, compression, delaying, advancing, and splitting, are achieved by the spectral tuning of the pulse carrier wavelength near surface plasmon resonances.

A DVD comprises a multilayer grating consisting of a polycarbonate substrate, a set of thin active layers, an intermediate reflective silver layer with a thickness of 50–100 nm, and a polycarbonate superstrate. Commercial discs have been proven to be a convenient medium for observing SPP resonances [30, 31]. The polycarbonate top layer was mechanically removed to observe SPPs at the air-metal interface. Studies of the remaining layers show that the DVD-based plasmonic crystal has a period of 750 nm and a modulation depth of 60 nm, as depicted in Fig. 1a.

The reflection spectra of the sample were measured for  $s$ - and  $p$ -polarized light. While no resonant features were detected for the  $s$ -polarized light, the reflection spectra, measured for the  $p$ -polarized light for different angles of incidence  $\theta$  shown in Fig. 1b have pronounced resonances related to the SPP excitation at the air-metal interface; their angular spectral position is associated with the SPP dispersion. Intersections of the dispersion curves achieved at normal light incidence and at  $\theta = 21^\circ$  lead to the formation of PBGs. The dispersion curves of the SPP excitation define the operating spectral range of the plasmon-based pulse shaper.

Two experimental configurations (described in Section 3) were considered for ultrafast studies. The first configuration is the case of  $\theta = 67^\circ$  with the single surface plasmon resonance located far from the PBGs, as shown in Fig. 1c. This configuration produces a

<sup>†</sup>The article is published in the original.

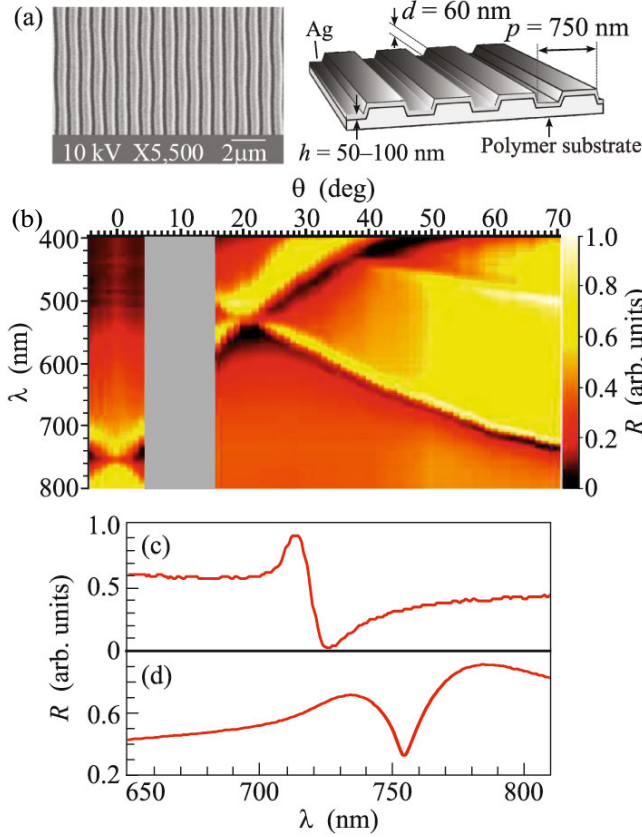


**Fig. 1.** (Color online) (a) Scanning electron microscopy image and scheme of the DVD-based plasmonic crystal sample. (b) Reflection coefficient of the plasmonic crystal versus the wavelength  $\lambda$  and angle of incidence  $\theta$  measured for  $p$ -polarized incident light. Data within the grey rectangle are not available. (c) Reflection spectrum for  $\theta = 67^\circ$ . (d) Reflection spectrum for  $\theta = 1^\circ$ .

Fano line shape caused by the interference of directly reflected light and the light reradiated by SPPs [32–34]. The reflectance  $R(\omega) = |r(\omega)|^2$  is represented by a complex sum of the nonresonant reflection of the incident radiation and the resonance profile of the SPP with a Lorentzian line shape:

$$r(\omega) = C_0 + \frac{f\Gamma e^{i\phi}}{\omega - \omega_R + i\Gamma}, \quad (1)$$

where  $C_0$  is the nonresonant reflection amplitude, which is considered independent of  $\omega$  because the nonresonant contribution varies insignificantly relative to the SPP-induced reflection modifications;  $f e^{i\phi}$  is the oscillator strength;  $\omega_R$  is the resonance frequency, and  $\Gamma$  is the SPP resonance width.

Another case comprises a PBG observed at the near-normal incidence found for  $\lambda = 750$  nm. The reflection spectrum shown in Fig. 1d is a superposition of two resonances with Fano-type line shapes. The bi-resonant shape of the spectrum makes it futile to attempt to determine the actual width of the PBG: the

resonant frequencies  $\omega_{R_{1,2}}$  for the PBG edges lie somewhere between the reflection maxima and minimum. Such a complex reflection spectra of the plasmonic crystal should lead to the pulse shaping of the reflected femtosecond laser pulses, which can be controlled by tuning the carrier wavelength or the angle of incidence.

## 2. CORRELATION FUNCTION MEASUREMENTS

The time-resolved response of the plasmonic crystal was studied using an intensity correlation function measurement setup based on a Ti:sapphire laser generating a train of 130 fs pulses; for details of the experimental setup, see [22]. The intensity correlation functions (CFs),  $I_{CF}(\tau)$ , were measured to determine the effect of the surface plasmons on the femtosecond pulse shape. Here,  $\tau$  is the time delay between the laser pulse reflected from the sample and the reference laser pulse. The measured correlation functions were compared using the autocorrelation functions (ACFs) obtained after azimuthally rotating the sample by  $90^\circ$ . Both the CFs and the ACFs were then fitted to the Gaussian function if possible, and the broadening and shifts of the CFs and ACFs were acquired. For the single resonance case, the electric fields were numerically reconstructed based on the Fano resonance model using the procedure described below.

The electric field amplitude of the laser pulse  $E_1(\omega)$  is modeled by a Gaussian function with the carrier frequency  $\omega_0$ , amplitude  $A_\omega$ , and pulse duration  $t_0$ . The electric field amplitude is described in the spectral domain as

$$E_1(\omega) = A_\omega e^{-t_0^2(\omega - \omega_0)^2/2}, \quad (2)$$

and in the time domain as

$$E_1(t) = A e^{-t^2/2t_0^2} e^{-i\omega_0 t}. \quad (3)$$

Equations (1) and (2) determine the electric field  $E_2(\omega)$  of the pulse reflected from the sample:

$$\begin{aligned} E_2(\omega) &= E_1(\omega)r(\omega) \\ &= A_\omega e^{-t_0^2(\omega - \omega_0)^2/2} \left( C_0 + \frac{f\Gamma e^{i\phi}}{\omega - \omega_R + i\Gamma} \right). \end{aligned} \quad (4)$$

According to the convolution theorem, this pulse has the following shape in the time domain:

$$\begin{aligned} E_2(t) &= \int_{-\infty}^{\infty} A e^{-t'^2/2t_0^2} \\ &\times e^{-i\omega_0 t'} \left( f\Gamma e^{i\phi - (i\omega_R + \Gamma)(t-t')} H(t-t') + C_0 \delta(t-t') \right) dt', \end{aligned} \quad (5)$$

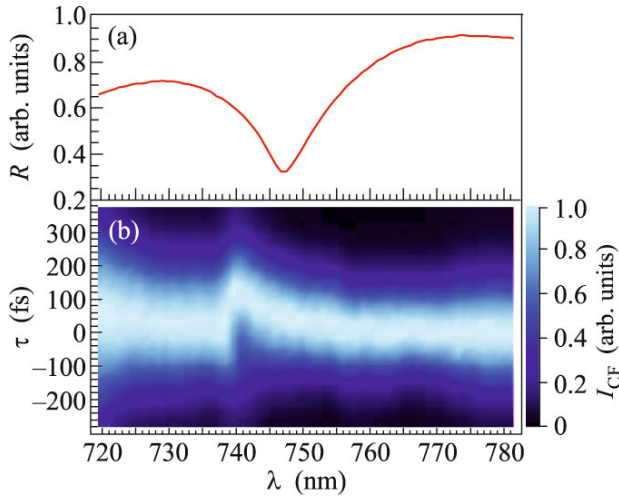


**Fig. 2.** (Color online) (a) Reflection coefficient for the plasmonic crystal sample as a function of wavelength  $\lambda$  measured for  $\theta = 1^\circ$ . (b) Experimental spectral dependence of the normalized correlation function in the spectral range of the plasmonic band gap.

where  $H(t)$  is the Heaviside step function. In the experiment, pulse  $E_2(t)$  was spatially combined at the nonlinear crystal with the reference laser pulse  $E_1(t)$  and the former was controllably delayed by  $\tau$  with respect to the latter. The measured intensity of the second-harmonic radiation is proportional to the second-order intensity correlation function:

$$I_{CF}(\tau) \sim \int_{-\infty}^{\infty} |E_1(\tau - t')|^2 |E_2(\tau')| dt'. \quad (6)$$

The fitting parameter set  $(\phi, A, f, \Gamma, \omega_R, C_0)$  can be adjusted to numerically evaluate Eq. (6) and fit it to the experimentally obtained correlation functions.

The spectral dependence of the CF measured for the carrier wavelength of fs-pulses,  $\lambda_0 = 2\pi c/\omega_0$ , tuned from 720 to 780 nm in 1 nm increments for the near-band-gap case is shown in Fig. 2b. Only a slight modification of the CF within the experimental uncertainties is observed for the long-wavelength resonance. This result means that the lifetime and/or amplitude of the SPP excitation are small relative to the nonresonant contribution. For the short-wavelength band-gap edge at  $\lambda_0 = 740$  nm, the CF is significantly modified, and the plasmonic impact becomes obvious. Broadening of the CF is detected in the spectral range from  $\lambda_0 = 733$  nm to  $\lambda_0 = 745$  nm, which is accompanied by a temporal shift of the CF maximum by up to 100 fs for  $\lambda_0 = 740$  nm. A series of CFs measured for six carrier wavelengths near the PBG edge as shown in Fig. 3 reveals a clear double-peaked pulse structure.

The scenario of envelope modification by  $\lambda_0$  tuning is developed as follows. First, the fs-pulse is broadened ( $\lambda_0 = 737, 738$  nm), and then a rise of the second peak

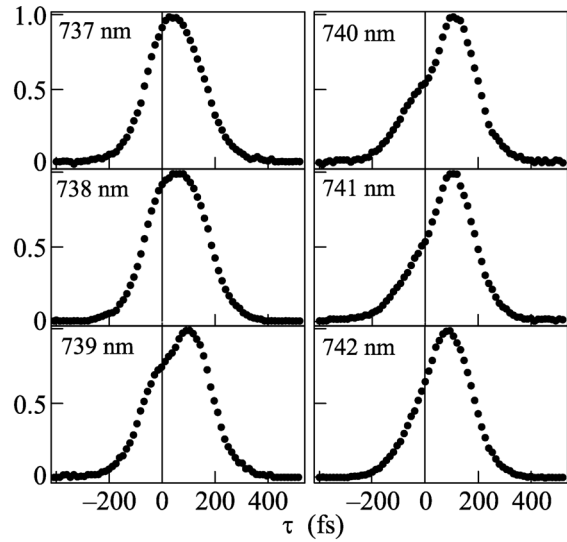
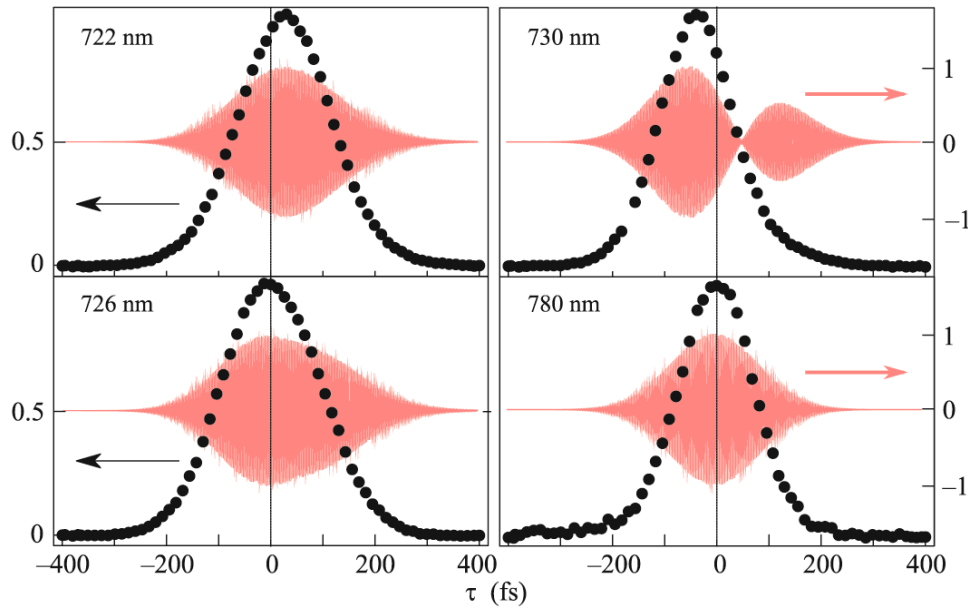


**Fig. 3.** Correlation functions measured for carrier wavelengths  $\lambda_0$  from 737 to 742 nm at the short wavelength band-gap edge,  $\theta = 1^\circ$ .

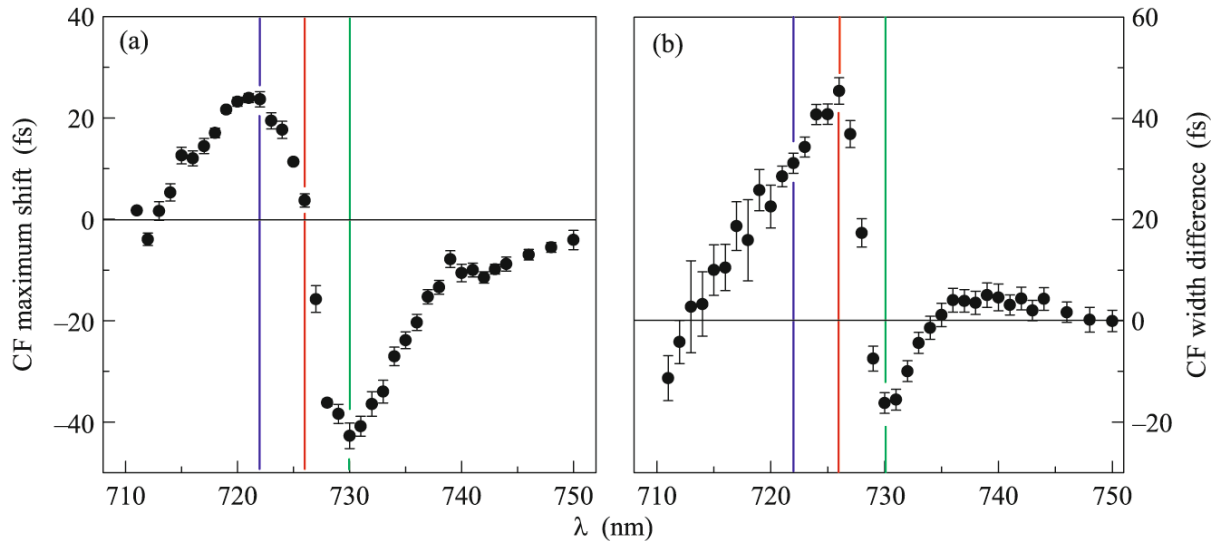
in the CF is observed for tuned from 739 to 741 nm. Finally, the width of the pulse returns to the initial laser pulse width at 745 nm. The appearance of the second peak in the CFs can be interpreted by the Fano resonance model of Eq. (1). It is a superposition of two processes: surface plasmon excitation and nonresonant reflection, with the former being slightly delayed relative to the latter because of the finite SPP lifetime. The influence of the second resonance of the band gap does not seem to cause these crucial pulse distortion effects, possibly due to the superradiation damping of this resonance [29].

Figure 4 shows the measured CFs and the reconstructed electric fields of the reflected pulses for an angle of incidence of  $\theta = 67^\circ$  and wavelengths far from PBGs. The CF profiles are described by the single Fano resonance model. For  $\lambda_0 = 722$  nm, the resonant component of the reflected pulse and the nonresonant pulse are in phase; they interfere constructively, broadening and delaying the reflected pulse  $E_2$ . For the Fano resonance minimum achieved at  $\lambda_0 = 730$  nm, the two components are out of phase and interfere destructively, producing a negative shift of the CF and a minimum of the  $E_2$  envelope the “zero-field” within the laser pulse. This is possible because of strong interplay between the two summands in Eq. (1), and this effect cannot be achieved for the sole Lorentzian resonance.

The spectral behaviors of the CF maximum and the CF width are summarized in Fig. 5. A delay of the CF by up to  $24 \pm 2$  fs is detected near the maximum of the reflection coefficient at  $\lambda_0 = 722$  nm. The broadening reaches the maximal value of  $45 \pm 2$  fs at  $\lambda_0 = 726$  nm. Near the Fano resonance minimum at  $\lambda_0 = 730$  nm, the CF is narrowed by  $16 \pm 2$  fs, and its maximum over-



**Fig. 4.** (Color online) Measured correlation functions and reconstructed pulses reflected from the sample for carrier wavelengths  $\lambda_0$  from 722 to 780 nm in the far-from-band-gap case and  $\theta = 67^\circ$ .



**Fig. 5.** (Color online) (a) Spectrum of the CF maximum shift with respect to the unperturbed pulse. Positive shifts indicate a temporal delay of the reflected pulse. (b) Spectrum of the CF broadening with respect to the unperturbed pulse. The spectra correspond to the far-from-band-gap case, with  $\theta = 67^\circ$ . Vertical lines denote the carrier wavelengths  $\lambda_0 =$  (blue line) 722, (red line) 726, and (green line) 730 nm.

takes the maximum of the unperturbed pulse by  $43 \pm 2$  fs.

We further explore the “zero-field” feature by visualizing it as a phase discontinuity in the traces of the short-time Fourier transform (STFT) obtained for the single Fano resonance. The STFT is a signal processing method for analyzing nonstationary signals with time-varying statistical characteristics and extracts several frames of the signal to be analyzed using a gate

function that moves in time. In our case, the gate function can be taken as  $E_{\text{gate}} = |E_1(t)|$ , i.e., as a Gaussian function envelope centered at  $\lambda_0$  with a duration equal to the laser pulse duration:

$$\text{STFT}(\tau, \omega) = \int_{-\infty}^{\infty} E_2(t') E_{\text{gate}}(t' - \tau) e^{i\omega t'} dt'. \quad (7)$$

Equation (7) allows the extraction of the time dependences of the intensity  $I$  and phase  $\Psi$  of each spectral component. Figure 6a shows the STFT time-resolved spectra of the unperturbed laser pulse with  $\lambda_0 = 800$  nm. The STFT image for intensity is circularly symmetric. The image for the pulse with  $\lambda_0 = 726$  nm is shown in Fig. 6b. There are slight changes in the STFT spectra: the long-wavelength components of the pulse are suppressed near  $\tau = 100$  fs. The STFT intensity spectra at  $\lambda_0 = 726$  nm shown in Fig. 6c corresponding to the wavelength of the Fano resonance minimum and the “zero-field” effect have a strong dip at  $\tau = 100$  fs near 730 nm. This feature indicates that, at this time delay, the spectral component of the carrier wavelength with maximal intensity within the incident laser pulse is suppressed due to destructive interference, which leads to an uncertainty in the phase at that moment and its discontinuity in the traces. This delay time is a moment of the “zero-field” of  $E_2$  in Fig. 4.

The right-hand column of Fig. 6 shows the time-resolved phase spectra of the reflected pulses. For the unperturbed pulse with  $\lambda_0 = 800$  nm, the phase image is symmetrical. The phase singularities are obtained at  $\tau = 100$  fs for  $\lambda_0 = 726$  nm and  $\lambda_0 = 730$  nm. Their spectral and time delay positions are the same as the dip positions in the STFT intensity spectra. For the single-resonance case, the SPP lifetime extracted from the reconstructed pulses is 43 fs, which is shorter than the laser pulse duration of 130 fs. The temporal pulse shape modifications are smaller than those for the near-band-gap case: compare the CF delay up to 100 fs for the band-gap case and from  $-40$  fs to 20 fs for the single-resonance case. However, due to the interplay between the background and the resonant contributions to the Fano-type line shape, the single-resonance case allows the pulse to be split into two, which is unattainable with a single Lorentz resonance.

Finally, note the possible improvements of this technique for more flexible pulse shaping. While the proposed nanostructure is indeed compact, it lacks adjustability relative to conventional pulse shapers. However, a serial combination of different gratings with different resonance profiles may lead to the miniaturization of pulse shaping devices.

In conclusion, femtosecond pulse shaping is realized in a 1D plasmonic crystal through experimental control of the ultrafast plasmonic optical response. Pulse stretching, compression, delay, advance, and splitting are shown to emerge in fs-pulses reflected from the plasmonic crystal. The particular effect on the pulse strongly depends on the carrier wavelength of the pulse and its spectral position with respect to the plasmonic Fano-type resonance. New opportunities for femtosecond pulse reshaping could be provided by more complex grating geometries, for example, with two-dimensional gratings or structures with chiral apertures or with stacks of plasmonic nanostructures with different parameters.

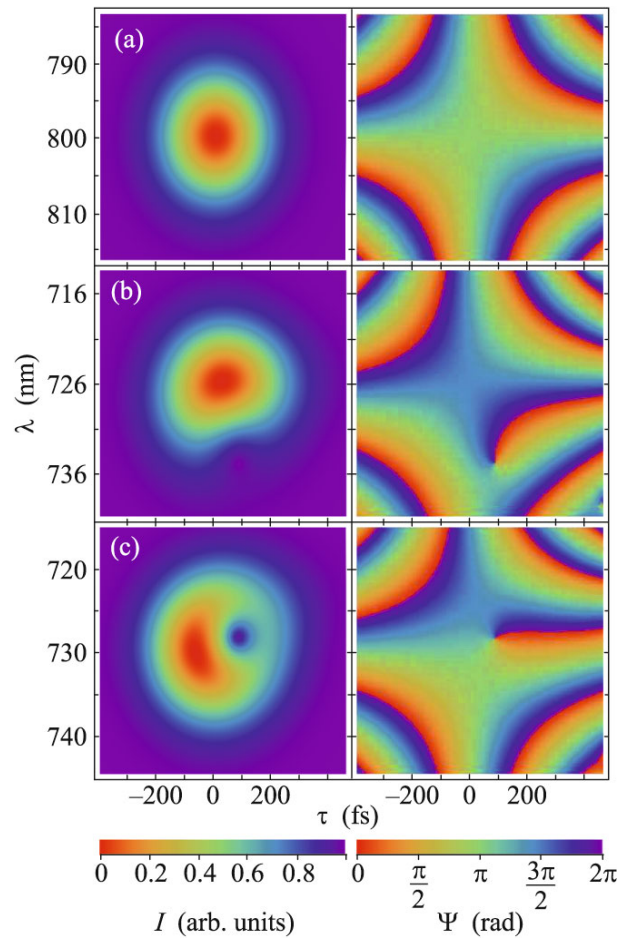


**Fig. 6.** (Color online) Short-time Fourier transform with a 130-fs-wide Gaussian gate-function. Left column: time-resolved intensity spectra of the reflected pulse. Right column: time-resolved phase spectra. (a) Reflected pulse far from resonance,  $\lambda_0 = 800$  nm. (b) Fano resonance curve inflection wavelength  $\lambda_0 = 726$  nm. (c) Fano resonance minimum wavelength  $\lambda_0 = 730$  nm.

This work was supported by the Russian Foundation for Basic Research and the Ministry of Education and Science of the Russian Federation (contract no. RFMEFI61314X0029).

## REFERENCES

1. A. Sharan and D. Goswami, *Curr. Sci.* **82**, 30 (2002).
2. A. M. Weiner, *Opt. Commun.* **284**, 3669 (2011).
3. Y. Silberberg, *Annu. Rev. Phys. Chem.* **60**, 277 (2009).
4. F. Frei, A. Galler, and T. Feurer, *J. Chem. Phys.* **130**, 034302 (2009).
5. D. Goswami, *Phys. Rep.* **374**, 385 (2003).
6. A. M. Weiner, Y. Silberberg, H. Fouckhardt, D. E. Leaird, M. A. Saifi, M. J. Andrejco, and P. W. Smith, *IEEE J. Quantum Electron.* **25**, 2648 (1989).

7. G. Tearney, M. Brezinski, B. Bouma, S. Boppart, C. Pitris, J. Southern, and J. Fujimoto, *Science* **276**, 2037 (1997).
8. F. Courvoisier, V. Boutou, V. Wood, A. Bartelt, M. Roth, H. Rabitz, and J. Wolf, *Appl. Phys. Lett.* **87**, 063901 (2005).
9. A. M. Weiner, Z. Jiang, and D. E. Leaird, *J. Opt. Netw.* **6**, 728 (2007).
10. L. Boivin, M. Wegmueller, M. Nuss, and W. Knox, *IEEE Photon. Technol. Lett.* **11**, 466 (1999).
11. E. Palushani, L. Oxenlowe, M. Galili, H. Mulvad, A. Clausen, and P. Jeppesen, *IEEE J. Quantum Electron.* **45**, 1317 (2009).
12. A. M. Weiner, *Rev. Sci. Instrum.* **71**, 1929 (2000).
13. A. Monmayrant and B. Chatel, *Rev. Sci. Instrum.* **75**, 2668 (2004).
14. T. Mansuryan, M. Kalashyan, J. Lhermite, E. Suran, V. Kermene, A. Barthelemy, and F. Louradour, *Opt. Lett.* **36**, 1635 (2011).
15. D. Leaird and A. Weiner, *Opt. Lett.* **24**, 853 (1999).
16. A. Vega, D. Leaird, and A. Weiner, *Opt. Lett.* **35**, 1554 (2010).
17. G. Dolling, C. Enkrich, M. Wegener, C. Soukoulis, and S. Linden, *Science* **312**, 892 (2006).
18. V. Fedorov and T. Nakajima, *Phys. Rev. Lett.* **107**, 143903 (2011).
19. R. Andaloro, H. Simon, and R. Deck, *Appl. Opt.* **33**, 6340 (1994).
20. A. Dogariu, T. Thio, L. J. Wang, T. W. Ebbesen, and H. J. Lezec, *Opt. Lett.* **26**, 450 (2001).
21. D. Kim, S. Hohng, V. Malyarchuk, Y. Yoon, Y. Ahn, K. Yee, J. Park, J. Kim, Q. Park, and C. Lienau, *Phys. Rev. Lett.* **91**, 143901 (2003).
22. P. P. Vabishchevich, V. O. Bessonov, F. Y. Sychev, M. R. Shcherbakov, T. V. Dolgova, and A. A. Fedyanin, *JETP Lett.* **92**, 575 (2011).
23. M. R. Shcherbakov, P. P. Vabishchevich, V. V. Komarova, T. V. Dolgova, V. I. Panov, V. V. Moshchalkov, and A. A. Fedyanin, *Phys. Rev. Lett.* **108**, 253903 (2012).
24. P. P. Vabishchevich, A. Y. Frolov, M. R. Shcherbakov, A. A. Grunin, T. V. Dolgova, and A. A. Fedyanin, *J. Appl. Phys.* **113**, 17A947 (2013).
25. M. R. Shcherbakov, P. P. Vabishchevich, A. Y. Frolov, T. V. Dolgova, and A. A. Fedyanin, *Phys. Rev. B* **90**, 201405(R) (2014).
26. W. L. Barnes, T. W. Preist, S. C. Kitson, and J. R. Sambles, *Phys. Rev. B* **54**, 6227 (1996).
27. S. I. Bozhevolnyi, V. S. Volkov, K. Leosson, and A. Boltasseva, *Appl. Phys. Lett.* **79**, 1076 (2001).
28. A. Vengurlekar, A. Gopal, and T. Ishihara, *Appl. Phys. Lett.* **89**, 181927 (2006).
29. C. Ropers, D. J. Park, G. Stibenz, G. Steinmeyer, J. Kim, D. S. Kim, and C. Lienau, *Phys. Rev. Lett.* **94**, 113901 (2005).
30. E. Fontana, *Appl. Opt.* **43**, 79 (2004).
31. A. A. Grunin, A. V. Chetvertukhin, T. V. Dolgova, A. A. Ezhov, and A. A. Fedyanin, *J. Appl. Phys.* **113**, 17A946 (2013).
32. U. Fano, *Ann. Phys.* **424**, 393 (1938).
33. C. Genet, M. P. van Exter, and J. P. Woerdman, *Opt. Commun.* **225**, 331 (2003).
34. A. E. Miroshnichenko, S. Flach, and Y. S. Kivshar, *Rev. Mod. Phys.* **82**, 2257 (2010).